Dyes and Pigments 185 (2021) 108897

Contents lists available at ScienceDirect

Dyes and Pigments

journal homepage: http://www.elsevier.com/locate/dyepig

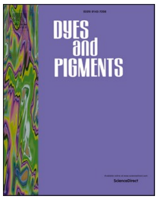

Multifunctional Porphyrin-based dyes for cations detection in solution and thermoresponsive low-cost materials

Nuno M.M. Moura [a,**], Simone Valentini [b,d], Victoria Cheptene [b,d], Andrea Pucci [d], M. Graça P. M.S. Neves [a], José Luis Capelo [b,c], Carlos Lodeiro [b,c], Elisabete Oliveira [b,c,*]

[a] LAQV-REQUIMTE, Department of Chemistry, University of Aveiro, 3810-193, Aveiro, Portugal
[b] BIOSCOPE Group, LAQV-REQUIMTE, Nova School of Science and Technology, NOVA University Lisbon, Caparica Campus, 2829-516, Caparica, Portugal
[c] ProteoMass Scientific Society, Madan Parque. Rua dos Inventores, 2825-182, Caparica, Portugal
[d] Department of Chemistry and Industrial Chemistry, Via Giuseppe Moruzzi 13, 56124, Pisa, University of Pisa, Italy

ARTICLE INFO

Keywords:
Porphyrins
Metal ions
Low-cost polymers
Temperature

ABSTRACT

Two β-pyrrolic substituted porphyrinic dyes **3** and **4,** have been synthesized and fully characterized. Both compounds showed spectral alterations upon metal interaction indicating the complexation of the inner nitrogens in the porphyrin moiety by the metal ion. Their sensing ability towards the divalent and monovalent, Zn^{2+}, Cd^{2+}, Co^{2+}, Fe^{2+}, Ni^{2+}, Cu^{2+}, Ag^{+} and Hg^{2+} metal ions was evaluated in solution by absorption and fluorescence spectroscopy. The association constants, minimal detectable and quantified amounts for all metal ions were also determined. The results reveal the formation of mononuclear species in all cases, with the best results obtained for the toxic Hg^{2+} metal ion, where the lowest detectable and quantified amounts of 0.9/5.3 μM and 1.8/3.6 μM were observed for compounds **3** and **4**, respectively. Polymeric films of poly(methylmethacrylate) (PMMA) doped with porphyrins **3** and **4** were also prepared and tested in the presence of the aforementioned metal ions and at different temperatures. For comparison, polymeric films of PMMA containing the non-substituted porphyrin 5,10,15,20-tetraphenylporphyrin (**TPP**) and with its Zn(II) complex (**ZnTPP**) were also tested at different temperatures. The temperature assays using the PMMA_**3** and PMMA_**4** doped polymers showed an interesting recovery in the emission intensity of *ca.* 70–80% in the cooling phase (from 100 °C to 35 °C). The results suggest the potential of these porphyrin dyes to be used in the preparation of smart plastic labels with temperature sensing features.

1. Introduction

During the last years, porphyrins and/or metalloporphyrins have been the target of several investigations for the development of new materials for multiple applications, mainly due to their unique variable optical and physical-chemical properties, which can be modulated by structural modifications of the tetrapyrrolic core [1]. In fact, these macrocycles adequately functionalyzed are being successfully applied in several areas, like catalysis, molecular sensing, artificial photosynthesis, chemotherapy, photodynamic therapy and molecular electronics [1–7].

Porphyrin compounds show remarkable photophysical properties, being visible excitable chromophores with characteristic absorption bands at *ca.* 400 nm (Soret) and at *ca.* 500–700 nm (Q-bands), large stokes shifts and emission bands longer than 600 nm, that minimizes the effects of the background fluorescence [1].

In free-base porphyrins, the *NH* inner groups and the size of the host cavity allow the complexation by metal ions affording metalloporphyrins, with different photophysical properties from the corresponding free base. The coordination of metal ions to the porphyrin macrocycle induces the formation of Lewis acid sites that can accommodate several ions and basic molecules as axial ligands. The complex formation is in general accompanied by a bathochromic shift of the Soret which is dependent on the ligand basicity and on the metal ion. Higher basicity of the ligands leads to higher stability constants and bathochromic shifts [8].

Because of such properties, the synthesis of adequately

---

* Corresponding author. BIOSCOPE Group, LAQV-REQUIMTE, Nova School of Science and Technology, NOVA University Lisbon, Caparica Campus, 2829-516, Caparica, Portugal.

** Corresponding author. LAQV-REQUIMTE, Department of Chemistry, University of Aveiro, 3810-193, Aveiro, Portugal.

E-mail addresses: nmoura@ua.pt (N.M.M. Moura), ej.oliveira@fct.unl.pt (E. Oliveira).

https://doi.org/10.1016/j.dyepig.2020.108897
Received 6 July 2020; Received in revised form 25 August 2020; Accepted 28 September 2020

functionalized porphyrins at *meso-* and β-pyrrolic positions and their potential to act as chemical probes for metal ions have been widely explored [1,9–11]. In this case, the porphyrin derivatives act as signalling unit based on the changes in the absorption and emission spectra. In previous works, Moura et al. reported the behaviour of a wide range of monomeric porphyrin derivatives in the presence of Ag^{+}, Cu^{2+}, Zn^{2+}, Cd^{2+} and Hg^{2+}. Some of those porphyrin derivatives revealed high selectivity to specific metal ions [12–15].

Another strategy that has been explored involves the immobilization of the porphyrin derivatives in other materials in order to enhance their reactivity to metal ions and other analytes [16–20]. Having this strategy in mind, Moura et al. developed low-cost polymers based on poly (methylmethacrylate) (PMMA) doped with porphyrin derivatives. These polymers were tested towards Zn^{2+} and Hg^{2+} metal ions. Similarly to what was observed in solution, the polymers showed a colour change from brown to green and emission quenching in the presence of these metal ions at room temperature (25 °C) [14]. Porphyrin derivatives have also been explored for the detection of microenvironments as pH and temperature [21,22]. Low-cost PMMA polymers were designed by Moura et al. using a porphyrin-chalcone derivative and tested at different temperatures (−20 °C, 25 °C, 50 °C), where an enhancement of the emission signal was visualized at −20 °C and 50 °C [12]. The doped polymers were further immersed in Zn^{2+}, and Hg^{2+} metal ions solutions, and similarly to what was observed in solution, an enhancement in the emission signal was detected at room temperature (25 °C). The same behaviour was observed at −20 °C and 50 °C. These preliminary results showed to be very promising molecules in the application of the low-cost polymers to measure temperatures in different ranges. Based on such results, herein we present the synthesis and characterization of two new cationic β-pyrrolic molecules **3** and **4**, and their sensing ability towards Zn^{2+}, Cd^{2+}, Co^{2+}, Fe^{2+}, Ni^{2+}, Cu^{2+}, Hg^{2+} and Ag^{+} metal ions. The ability of these probes was also evaluated in solid state by preparing several PMMA films doped with both ligands, **3** and **4**. The resulting doped films were explored towards metal ions and with temperature variation studies (heating from 25 °C to 100 °C and cooling from 100 °C to 35 °C). As reference samples, we have used the non-substituted template 5,10,15,20-tetraphenylporphyrin (**TPP)** and its Zn(II) complex **ZnTPP.**

2. Experimental section

2.1. Chemicals and starting materials

Iron(II) perchlorate hydrate (>98%), Cobalt(II) trifluoromethanesulfonate (>98%), Cadmium(II) trifluoromethanesulfonate (>98%), Mercury(II) trifluoromethanesulfonate (>98%), Copper(II) trifluoromethanesulfonate (>98%), Zinc(II) trifluoromethanesulfonate (>98%), Silver(I) trifluoromethanesulfonate (>98%) and Nickel(II) trifluoromethanesulfonate (>98%) were purchased from Solchemar. Poly (methyl methacrylate) (PMMA, Mw = 350,000 g/mol, acid number <1 mg KOH/g) and all solvents were from Sigma Aldrich. All chemicals and solvents were used without further purification.

2.2. General remarks

^{1}H and ^{13}C solution NMR spectra were recorded on Bruker Avance 300 (300.13 and 75.47 MHz, respectively) and Avance 500 (500.13 and 125.76 MHz, respectively) spectrometers. CDCl$_3$ was used as solvent and tetramethylsilane (TMS) as the internal reference; the chemical shifts are expressed in δ (ppm) and the coupling constants (J) in Hertz (Hz). Unequivocal ^{1}H assignments were made using 2D COSY (^{1}H/^{1}H), while ^{13}C assignments were made based on 2D HSQC (^{1}H/^{13}C) and HMBC (delay for long-range $J_{C/H}$ couplings were optimized for 7 Hz) experiments. Electrospray ionization mass spectra were acquired with a Micromass Q-Tof 2 (Micromass, Manchester, UK), operating in the positive ion mode, equipped with a Z-spray source, an electrospray probe and a syringe pump. Source and desolvation temperatures were 80 °C and 150 °C, respectively. Capillary voltage was 3000 V. The spectra were acquired at a nominal resolution of 9000 and at cone voltages of 30 V. Nebulisation and collision gases were N$_2$ and Ar, respectively. Porphyrin solutions in methanol were introduced at a 10 μL min^{-1} flow rate. Mass spectra HRMS were recorded on a LTQ Orbitrap XL mass spectrometer (Thermo Fischer Scientific, Bremen, Germany) using methanol as solvent. Column chromatography was carried out using silica gel (Merck, 35–70 mesh). Analytical TLC was carried out on precoated sheets with silica gel (Merck 60, 0.2 mm thick). All the chemicals were used as supplied. Solvents were purified or dried according to the literature procedures [23].

2.3. Synthesis of ligands

2.3.1. Synthesis of 5,10,15,20-tetraphenylporphyrin (TPP) and (5,10,15,20-tetraphenylporphyrinato)zinc(II) (ZnTPP)

TPP was prepared in 28% yield by condensation of pyrrole and benzaldehyde following an adaptation of the well-established Adler protocol [24–26]. **ZnTPP** was obtained by metalation of the free-base **TPP** with the adequate metal carrier, zinc(II) acetate, according to conventional procedures [27]. The structures of **TPP** and **ZnTPP** were confirmed by ^{1}H NMR, mass spectrometry and UV–vis techniques. The experimental data are in agreement with the one described in the literature.

5,10,15,20-Tetraphenylporphyrin (TPP) - ^{1}H NMR (300 MHz, CDCl$_3$): δ 8.85 (8H, s, H-β), 8.23–8.20 (8H, m, H-*o*-Ph), 7.78–7.66 (12H, m, H-*m,p*-Ph), −2.77 (2H, s, *N*-H) ppm. **MS-ESI(+)**: *m/z* 614.2 [M]$^{+\cdot}$. **UV–vis** (DMF): $\lambda_{\max}$ (log ε) 416 (5.27), 512 (4.09), 546 (3.75), 590 (3.57), 647 (3.55) nm.

(5,10,15,20-Tetraphenylporphyrinato)zinc(II) (ZnTPP) - ^{1}H NMR (300 MHz, CDCl$_3$): δ 8.95 (8H, s, H-β), 8.24–8.21 (8H, m, H-*o*-Ph), 7.81–7.70 (12H, m, H-*m,p*-Ph) ppm. **MS-ESI(+)**: *m/z* 676.3 [M]$^{+\cdot}$. **UV–Vis** (DMF): $\lambda_{\max}$ (log ε) 424 (5.99), 559 (4.58), 597 (4.24) nm.

2.3.2. Synthesis of porphyrinic derivatives 1 and 2

The benzoporphyrin **1** and porphyrin-chalcone type **2** derivatives were obtained through an aldol-type reaction by reaction of 2-formyl-5,10,15,20-tetrapenhylporphyrin with the adequate 3-acetylpyridine according to previously described procedures [28,29]. The reactions were performed in dry toluene in the presence of catalytic amounts of lanthanum(III) trifluoromethanesulfonate (La(OTf)$_3$), using ammonium acetate [28] or piperidine [29] as base.

2.3.3. Synthesis of porphyrinic derivatives 3 and 4

To a solution of benzoporphyrin **1** or porphyrin-chalcone derivative **2** in *N,N*′-dimethylformamide (1 mL) was added sodium iodide and *S*-(4-bromobutyl)thioacetate and the mixture was stirred for 22 h at 120 °C. After cooling, the reaction mixture was washed with water and extracted with dichloromethane. The organic phase was dried (Na$_2$SO$_4$) and the solvent was evaporated under reduced pressure. The crude mixture was submitted to column chromatography (silica gel) using dichloromethane/methanol (98:2) as the eluent. The fractions obtained were fully characterized by NMR, mass and spectroscopic techniques after crystallization in a CH$_2$Cl$_2$/hexane mixture.

2^{2}- [1-(4-(acetylthio)butyl)-pyridinium-3-yl] -5,10,15,20-tetraphenylbenzo [*b*] porphyrin iodide, *3*.

Yield: 95%. **^{1}H NMR** (500 MHz, CDCl$_3$): δ 9.55 (1H, d, $J = 5.8$ Hz, H-$2''$), 9.22 (1H, s, H-3), 8.94 (1H, d, $J = 4.9$ Hz, H-β), 8.91 (1H, d, $J = 4.9$ Hz, H-β), 8.87 (1H, d, $J = 4.9$ Hz, H-β), 8.75–8.71 (4H, m, H-β. H- $4''$ and H-$6''$), 8.25–8.19 (8H, m, H-*o*-Ph), 8.15 (1H, d, $J = 8.4$ Hz, H-$3'$), 8.10 (1H, dd, $J = 6.1$ and 7.9 Hz, H-$5''$), 7.95 (1H, t, $J = 7.6$ Hz, H-*p*-Ph), 7.89–7.64 (12H, m, H-*m,p*-Ph and H-$1'$), 7.43 (1H, d, $J = 8.4$ Hz, H-$4'$), 5.11 (2H, t, $J = 7.8$ Hz, H-$1'''$), 3.03 (2H, t, $J = 7.6$ Hz, H-$4'''$), 2.35 (3H, s, -CH_3), 2.25–2.19 (2H, m, H-$2'''$), 1.79 (2H, q, $J = 7.6$ Hz, H-$3'''$), −2.69 (2H, s, *N*-H) ppm. **^{13}C NMR** (125 MHz, CDCl$_3$): δ 196.4, 159.7, 155.3, 146.4, 145.9, 145.7, 143.9, 143.6, 142.7, 142.0, 141.69, 141.66, 141.58, 140.3, 139.9, 138.9, 138.4, 138.3, 135.4, 134.53, 134.50, 134.45, 134.41, 133.7, 133.5, 129.2, 128.3, 128.2, 128.1, 128.0, 127.1, 126.91, 126.89, 126.86, 121.7, 121.6, 118.4, 118.0, 117.2, 61.2, 31.0, 30.8, 28.1, 26.4 ppm. **MS-ESI(+)**: *m/z* 873.3 $[M+H]^+$. **HRMS-ESI**(+): *m/z* calculated to $C_{59}H_{47}N_5OS$ $[M+H]^+$ 873.3496; found 873.3344. **UV–Vis** (CH_2Cl_2): λ_{max} (log ε) 430 (5.0), 525 (4.0), 600 (3.6) nm.

2-[3-Oxo-3-(**1-(4-(acetylthio)butyl)**-pyridin-3-yl)propan-1-yl]-**5,10,15,20-tetraphenylporphyrin iodide**, **4**.

Yield: 87%. **^{1}H NMR** (500 MHz, $CDCl_3$): δ 10.07 (1H, d, $J = 4.9$ Hz, H-2″), 9.28–9.25 (2H, m, H-β), 8.85–8.76 (7H, m, H-β, H-4″ and H-6″), 8.25–8.13 (9H, m, H-*o*-Ph and H-5″), 7.85–7.62 (14H, m, H-*m,p*-Ph H-1′ and H-2′), 5.10 (2H, t, $J = 7.6$ Hz, H-1‴), 2.96 (2H, t, $J = 7.6$ Hz, H-4‴), 2.21 (3H, s, -CH_3), 2.18–2.15 (2H, m, H-2‴), 1.79 (2H, q, $J = 7.6$ Hz, H-3‴), −2.52 (2H, s, *N*-H) ppm. **^{13}C NMR** (125 MHz, $CDCl_3$): δ 197.1, 183.9, 145.9, 143.8, 141.8, 141.71, 141.65, 141.5, 137.6, 134.7, 134.6, 134.5, 133.8–129.5 (C-β), 128.9, 128.8, 128.2, 128.0, 127.3, 127.0, 126.91, 126.85, 121.4, 120.6, 120.0, 61.8, 30.7, 30.1, 27.5, 26.2 ppm. **MS-ESI(+)**: *m/z* 876.3 $[M]^+$. **HRMS-ESI**(+): *m/z* calculated to $C_{59}H_{46}N_5O_2S$ $[M]^+$ 876.33367; found 876.3352. **UV–Vis** (CH_2Cl_2): λ_{max} (log ε) 420 (4.9), 530 (3.4), 600 (3.3), 675 (3.1) nm.

2.4. Spectrophotometric and spectrofluorimetric measurements

UV–Vis absorption spectra were recorded with a JASCO V-650 spectrophotometer and a fluorescence emission by a HORIBA Scientific FLUOROMAX-4 spectrofluorimeter from the PROTEOMASS Scientific Society facility. The linearity of the fluorescence emission *vs.* the concentration was checked out in the concentration used (10^{-4} – 10^{-6} M). A correction for the absorbed light was performed when necessary. Spectra of solid samples were recorded on the Horiba-Jobin-Yvon Fluoromax-4® spectrofluorimeter using a fiber-optics device connected to the spectrofluorimeter, exciting the solid compounds at appropriated λ (nm).

2.4.1. Photophysical characterization and titrations

1 mg of fluorophore powder was weighted and solubilized in 5 mL of dichloromethane obtaining a 10^{-3} fluorophore stock solution. A 3 mL cuvette of 1×10^{-5} M fluorophore solution in dichloromethane was then prepared from the stock solution.

The stock solutions of the metal ions (*ca.* 10^{-2} M) were prepared by dissolving an appropriate amount of the corresponding cation salt derivative in acetonitrile (3 mL). The volumes corresponding to the desired cation equivalents were taken by the stock solutions using a micropipette, and added step by step to the cuvette containing the fluorophore solution in dichloromethane. The optical changes in absorption and emission spectra were collected after each addition. The measurement was carried until a *plateau* is reached in the spectra collected. All measurements were performed at 298 K and the metal ions tested were: Zn^{2+}, Cd^{2+}, Co^{2+}, Fe^{2+}, Ni^{2+}, Cu^{2+}, Hg^{2+} and Ag^+.

Luminescence quantum yields were measured using a solution of cresyl violet in ethanol [$\varphi_F = 0.54$] as a standard for compounds **3** and **4** [30,31]. All solvents used were of the highest purity from Merck.

2.5. Determination of the detection and quantification limits (LOD and LOQ)

The detection limit (LOD) and quantification limit (LOQ) are the lowest concentration level that can be detected and quantified to be statistically different from a blank. For the determination of LOD and LOQ, ten different measurements of a solution containing the selected probe were collected without the addition of any metal ion (y_{blank}). The LOD and LOQ were determined by the formulas:

LOD = y_{dl} = yblank + 3std, where ydl = signal detection limit and std = standard deviation.

LOQ = ydl = y_{blank} + 10std, where y_{dl} = signal detection limit and std = standard deviation.

Additionally, small amounts of the metal ions were added to a solution of porphyrins **3** or **4** in order to determine the minimal detectable and quantified concentration out of the LOD and LOQ values, respectively.

2.6. Preparations of thin polymeric films for sensing

Polymeric films were obtained at room temperature and under air ambient by dissolving 100 mg of PMMA in dichloromethane followed by the addition of the appropriated amount of each dye, in a dye/polymer ratio (% w/w) of 0.5, 1.5 and 3.0 for **TPP** and **ZnTPP**; 0.25, 0.5 and 1.5 for compounds **3** and **4**. Solid polymeric films with an average thickness of 9 μm were obtained by pouring each above-mentioned solution in an aluminium dish covered with a glass watch and keeping them under a hood at room temperature until complete solvent evaporation (about one day).

The obtained films were then cut in 10 × 15 mm rectangular pieces.

2.6.1. Chemical recognition

It was prepared a 10^{-2} M stock solution of the corresponding cation by the dissolution of the right amount of cation derivative powder in the wanted volume of water. The wanted volume of such solution was then withdrawn and opportunely diluted for the preparation of 5 vials each of them containing a different concentration of the cation. The cation involved were Zn^{2+}, Hg^{2+}, Cd^{2+}, and the concentration of each solution was varied in a range between 1.0×10^{-6} and 8×10^{-5} M.

The 10 × 15 mm rectangular samples were immersed in each of the solutions at different cation concentration previously prepared for around 5 min and then dried for removing the excess of the solution on the film surface. Optical changes in the absorption and emission spectra were collected. If any changes in the optical properties of the film were visualized, the measurement protocol were repeated three times.

2.6.2. Temperature sensing

The 10 × 15 mm rectangular samples were placed between two quartz slides and then positioned on support centred below the light spot of the optical fiber directly connected with the spectrophotometer. The support was replaced by the black plate of a heater. The heat was provided by the heater equipped with a thermostat (±1 °C) capable of maintaining the temperature stable during the optical analyses of the samples. The reaching of the desired temperature was registered by a digital temperature probe directly connected with the plate of the heater. The measures were performed from 25 to 100 °C and from 100 to 35 °C. Optical changes in the emission spectra were collected.

3. Results and discussion

3.1. Synthesis

The synthetic strategy to prepare the new ligands **3** and **4** is outlined in Scheme 1 and required a previous preparation of the corresponding of benzoporphyrin **1** and of porphyrin **2** bearing a chalcone-type unit. These derivatives were obtained through an aldol-type condensation involving the easily accessible 2-formyl-5,10,15,20-tetraphenylporphyrin and 3-acetylpyridine in the presence of catalytic amounts of La$(OTf)_3$ [28,29]. The 2-formyl-5,10,15,20-tetraphenylporphyrin was obtained by Vilsmeier-Haack formylation of 5,10,15,20-tetraphenylporphyrin (**TPP**) [32]. Further reaction of derivatives **1** and **2** with *S*-(4-bromobutyl)thioacetate in DMF at 120 °C (Scheme 1) afforded, after workup and purification by column chromatography, the new *beta*-functionalized mono-charged derivatives **3** (95%) and **4** (87%) in excellent yields. The structures of all compounds were unambiguously confirmed by 1D, and 2D NMR studies and their molecular formulas were confirmed by HRMS (see Supporting Information, Figs. S1–S14).

The ^{1}H NMR spectra of compounds **3** and **4** clearly shows in the

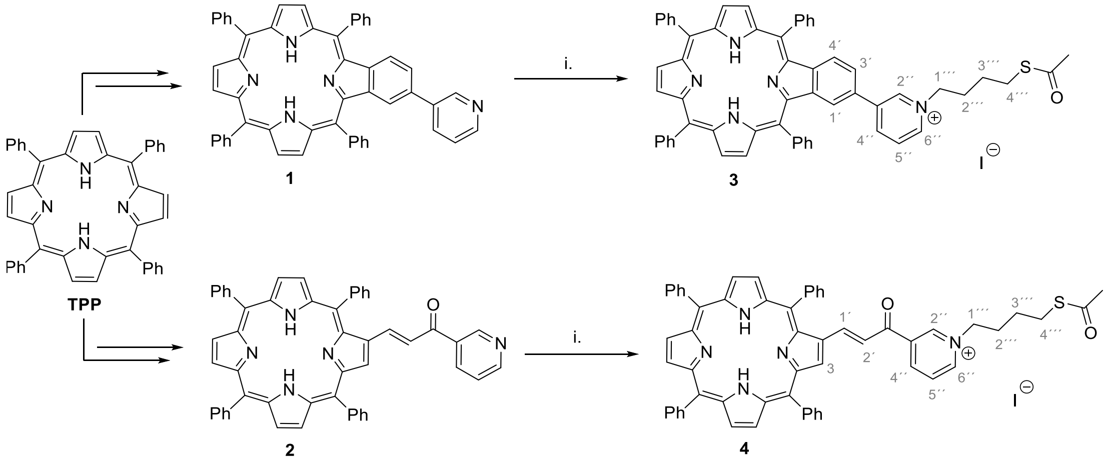

i. *S*-(4-Bromobutyl)thioacetate, NaI, DMF, 120 °C.

Scheme 1. Synthesis of ligands **3** and **4**.

aliphatic region, from *ca.* δ 5.1 ppm to δ 1.8 ppm, the peaks due to the resonances of the protons from the butyltioacetate unit attached to the pyridine moiety. The singlets at $\delta - 2.52$ ppm and $\delta - 2.69$ ppm, corresponding to the resonances of inner core *N*-H, demonstrates that both derivatives (**3** and **4**) are in their free-base form (see SI, Figs. S1 and S8). The ^{13}C NMR spectrum of compound **3** show a distinctive signal at δ 196.4 ppm corresponding to the carbonyl carbon of the butyltioacetate unit, while the ^{13}C NMR spectrum of the porphyrin-chalcone type derivative **4** presents two signals at δ 197.1 ppm and δ 183.9, due to the resonance of the carbonyl carbons of the butyltioacetate unit and chalcone moiety, respectively (see SI, Figs. S5 and S12).

3.2. *Photophysical characterization*

The absorption, emission and excitation spectra of the fluorophores **3** and **4** were performed in dichloromethane solutions at 298 K and are pesented in Fig. 1. Although the photophysical characterization of references 5,10,15,20-tetraphenyl-porphyrin (**TPP**) and of its Zn(II) complex **ZnTPP** are well described in literature [12,14,15,33], we decided, for comparison, to present in the same figure their absorption, emission and excitation spectra.

The absorption spectrum of **TPP** (Fig. 1A) shows the expected feature of a free-base porphyrin: the highly intense peak corresponding to the Soret or B band at 415 nm ($\varepsilon = 1 \times 10^6$ M^{-1} cm^{-1}) and the four weak Q bands in the range 500–700 nm [33]. Both B and Q bands in the visible range are assigned to π–π^* transitions, where the Soret band involves the

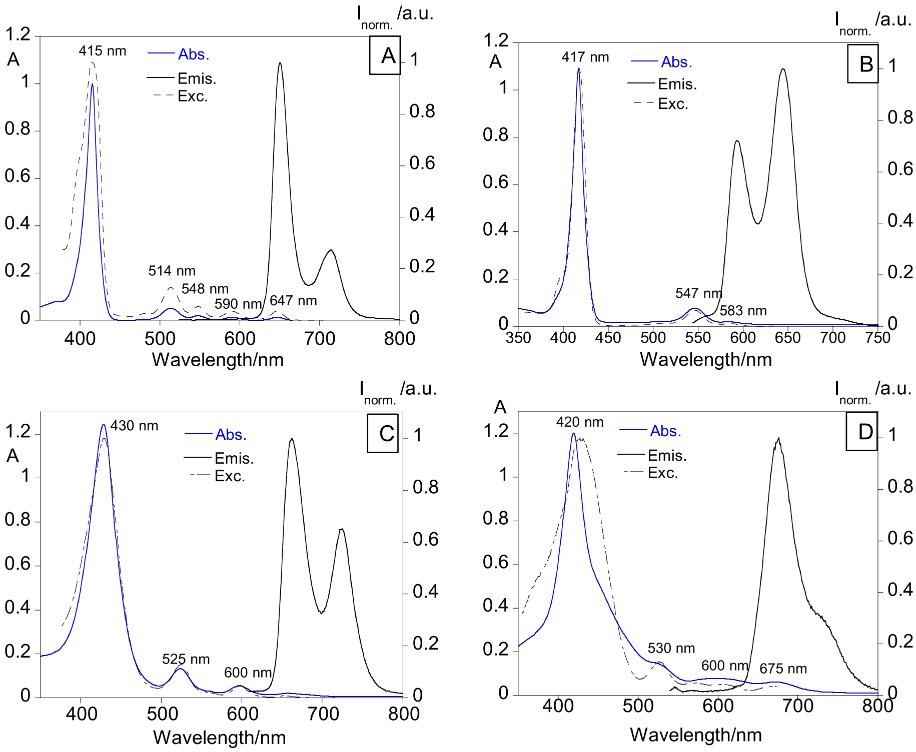

Fig. 1. Absorption, emission and excitation spectra of compounds **TPP** (A), **ZnTPP** (B), **3** (C) and **4** (D) in dichloromethane (*ca.* 10^{-5} M) at 298 K, $\lambda_{excTPP} = 548$ nm, $\lambda_{excZnTPP} = 547$ nm, $\lambda_{exc3} = 525$ and $\lambda_{exc4} = 530$ nm.

transition from the ground state to the second excited state (S_0–S_2) while the Q bands stem from a weak transition to the first excited state (S_0–S_1) in agreement with the Gouterman Four-Orbital Model prevision [34].

The absorption spectrum of **ZnTPP** (Fig. 1B) obtained by metalation of the free-base **TPP** with the adequate metal carrier, zinc(II) acetate, according to conventional procedures [4], presents the Soret band at around 417 nm ($\varepsilon = 1.1 \times 10^6$ M^{-1} cm^{-1}) accompanied by only two Q bands. This reduction in the number of bands from four to two is related with the alteration in the symmetry of the molecule from D_{2h} (properly of the free-base porphyrin) to D_{4h} with the consequent simplification of the absorption spectra in the Q region [35].

The absorption spectrum of **3** (Fig. 1C) shows highly intense Soret band peaked at 430 nm ($\varepsilon = 1.2 \times 10^5$ M^{-1} cm^{-1}), i.e. 15 nm red-shifted with respect to **TPP**, and flanked by only two discernible Q bands between 525 and 600 nm. The red-shift of the Soret band could be related to the presence of the six-membered fused aromatic ring in β-position on the porphyrin macrocycle capable of enhancing the π electrons delocalization.

In the case of compound **4** (Fig. 1D), the Soret band appears at 420 nm ($\varepsilon = 1 \times 10^5$ M^{-1} cm^{-1}), with a negligible red shift compared to **TPP** and with larger and partially overlapped Q bands. Moreover, the Soret band presents a not well-defined shape with a shouldered peak red-shifted at around 490 nm, a symptom of the possible coexistence of aggregates. In literature, it is reported that significant changes in the UV–Vis spectrum of porphyrins are promoted by increasing their concentration since aggregation phenomena can occur [36]. Notably, the broadening of the Soret band is detectable at a concentration higher than 5×10^{-5} M for **TPP**. This phenomenon could be more likely favored by the presence of the peripheric chain in compound **4** positively charged. This structural feature may increase the aggregation tendency of this porphyrin derivative in dichloromethane due to its higher amphiphilic behaviour that probably leads to the formation of cation-π dimers.

As shown in Fig. 1, the emission spectrum of fluorophore **3** present two well-defined peaks placed in the range 650–750 nm, which are characteristic of porphyrin derivatives. The emission spectrum of compound **4** presents a single enlarged band that is probably due to the partial overlapping of the two canonical peaks.

The fluorescence quantum yield (φ) determined by using a solution of crystal violet in methanol as a standard (φ = 0.54). The value obtained for **TPP** (φ = 0.11) was in accordance with the data reported in literature [14] and was higher than the ones obtained for derivatives **3** (φ = 0.012) and **4** (φ = 0.001).

3.3. *Metal sensing in solution*

The sensorial ability of porphyrins **3** and **4** towards transition and post-transitions metal ions (Zn^{2+}, Cd^{2+}, Co^{2+}, Fe^{2+}, Ni^{2+}, Cu^{2+}, $Hg^{2+}$and Ag^{+}), was determined by titrating the respective dichloromethane solutions, with small amounts of the metal ion in acetonitrile. The absorption and emission spectra were collected after every addition at 298 K until a *plateau* of the optical signal was reached. The stability constants of the interaction with all the investigated metal ions were calculated by using the HypSpec software [37].

3.3.1. *Zn^{2+} metal ion titration*

The addition of Zn^{2+} metal ions to compounds **3** and **4** promoted significant changes in the ground and excited states (Fig. 2). In all cases, a red shift of the Soret band (*ca.* 25 nm) was observed in the absorption spectra due to the interaction of Zn^{2+} metal ions with the electron lone-pair of the inner N atoms of the porphyrin macrocycle. The red shift is more intense in compound **3** than in **4**, with the formation of a new band at 455 nm. Interestingly, an isosbestic point is observed at 440 nm and 430 nm for **3** and **4**, respectively, confirming the presence of only two species in solution, the ligand and the metal complex. In the Q region is observed a decrease in the absorption at 525–530 nm, with the appearance of a new band at 670–675 nm for compounds **3** and **4**, respectively. The changes observed in the absorption spectra upon interaction with Zn^{2+} were also accompanied by a change of colour from pale yellow to green (Figure. 2A). These alterations are in line with the formation of a sitting-atop (SAT) complex in which the metal lies above the porphyrin plane with the two inner *N*-H protons still present [38–40]. Therefore, the second step involving the incorporation of the metal into the macrocycle core accompanied by the loss of two *N*-H protons was not observed under these titration conditions (see Fig. 2c for **ZnTPP**).

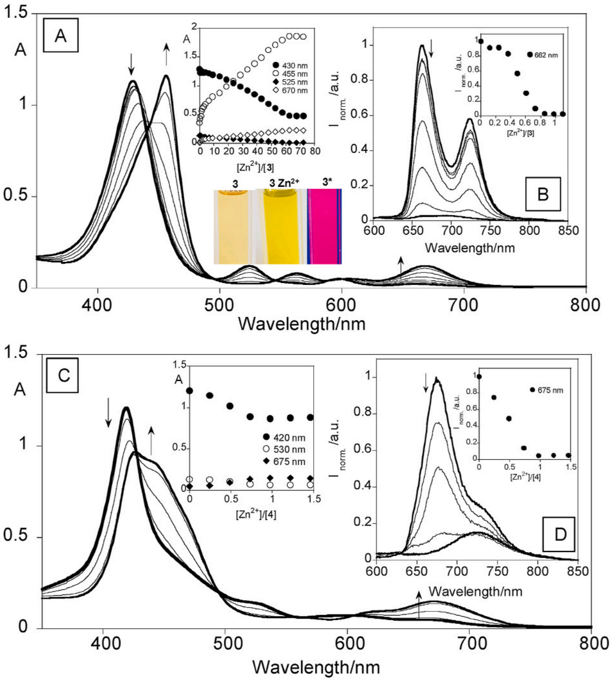

Fig. 2. Spectrophotometric (A and C) and spectrofluorimetric (B, D) titrations of compound **3** (A, B) and **4** (C,D) with the addition of Zn^{2+} in dichloromethane. The inset represents the absorption (A, C) at 430 nm, 455 nm, 525 nm, 670 nm for (A) and 420 nm, 530 nm, 675 nm for (C); and the emission intensity (B, D) at 662 nm (B) and 675 nm (D), as function of $[Zn^{2+}]/[\mathbf{3}]$ (A, B) and $[Zn^{2+}]/[\mathbf{4}]$ (C, D). Inset Fig. 3A: Naked-eye images of **3** before and after titration (**3**, **3**Zn^{2+}) and under a UV-lamp before titration (**3***). ([**3**], [**4**] = 1×10^{-5} M, $\lambda_{exc3} = 525$ nm, $\lambda_{exc4} = 530$ nm, T = 298 K).

Concerning the emission spectra in both compounds a quenching of the emission signal at *ca.* 662–675 nm (**3**, **4**) and at *ca.* 730 nm was observed, due to the free-base porphyrin emission Q (0-0) and Q(0–1) [41].

The stability constants were calculated for both compounds (Table 1), and all values revealed a stoichiometry 1:1 ligand-to-metal (L:M) in all cases. Respectively, values of Log $K_{ass} = 6.86 \pm 0.02$ (**3**) and Log $K_{ass} = 8.11 \pm 0.02$ (**4**) were determined.

3.3.2. *Cu^{2+} and Fe^{2+} metal ions*

The titration of compounds **3** and **4** with Cu^{2+} metal ions led to a red shift in the absorption bands. It was observed a decrease in the Soret band at 430 nm and 420 nm, followed by an absorption increase at 455 nm and 450 nm, and the formation of an isosbestic point at 440 and 430 nm for **3** and **4**, respectively (Fig. 3). In the Q bands, the same behaviour was detected with a decrease in the absorption band at 525 nm for derivative **3** and at 530 nm for **4** accompanied respectively by the appearance of new bands at 670 nm (**3**) and 675 nm (**4**). As can be seen in Fig. 4 the interaction with Cu^{2+} is stronger in compound **3**, being necessary a less amount of the metal ion to produce the spectral alterations. This result is in agreement with the obtained association constants with values of Log $K_{ass} = 7.58 \pm 0.11$ (**3**) and Log $K_{ass} = 6.25 \pm$

Table 1
Stability association constants and stoichiometry for the complexes formed with porphyrin derivatives **3** and **4** in dichloromethane with Zn^{2+}, Cd^{2+}, Co^{2+}, Fe^{2+}, Ni^{2+}, Cu^{2+}, Hg^{2+}, Ag^{+} ions (CH_3CN), (σ is an estimate of the average experimental error).

Compounds (L)	Metal (M)	Association constants ($LogK_{ass}$), σ L:M
3	Zn^{2+}	6.86 ± 0.02 (1:1)
	Cd^{2+}	6.52 ± 0.01 (1:1)
	Co^{2+}	4.85 ± 0.01 (1:1)
	Fe^{2+}	6.63 ± 0.15 (1:1)
	Ni^{2+}	5.36 ± 0.05 (1:1)
	Cu^{2+}	7.58 ± 0.11 (1:1)
	Hg^{2+}	7.75 ± 0.02 (1:1)
	Ag^{+}	2.49 ± 0.03 (1:1)
4	Zn^{2+}	7.11 ± 0.02 (1:1)
	Cd^{2+}	7.40 ± 0.02 (1:1)
	Co^{2+}	7.22 ± 0.05 (1:1)
	Fe^{2+}	6.62 ± 0.03 (1:1)
	Ni^{2+}	5.78 ± 0.01 (1:1)
	Cu^{2+}	6.25 ± 0.04 (1:1)
	Hg^{2+}	7.38 ± 0.04 (1:1)
	Ag^{+}	5.25 ± 0.01 (1:1)

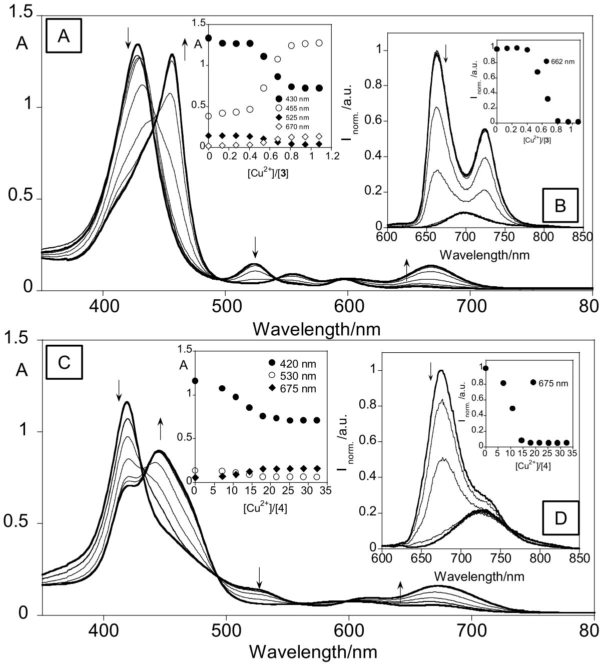

Fig. 3. Spectrophotometric (A, C) and spectrofluorimetric (B, D) titrations of compound **3** (A, B) and **4** (C,D) with the addition of Cu^{2+} in dichloromethane. The inset represents the absorption (A, C) at 430 nm, 455 nm, 525 nm, 670 nm for (A) and 420 nm, 530 nm, 675 nm for (C); and the emission intensity (B, D) at 662 nm (B) and 675 nm (D), as function of $[Cu^{2+}]/[\mathbf{3}]$ (A, B) and $[Cu^{2+}]/[\mathbf{4}]$ (C, D). ($[\mathbf{3}]$, $[\mathbf{4}] = 1 \times 10^{-5}$ M, $\lambda_{exc3} = 525$ nm, $\lambda_{exc4} = 530$ nm, T =

0.04 (**4**) for a stoichiometry of 1:1 (L:M). Both compounds exhibit a fluorescence quenching upon the binding of Cu^{2+}. In the case of Cu^{2+}, the quenching of the emission signal is attributed to its paramagnetic nature, which leads to non-radiative deactivation processes [42,43].

The titrations with Fe^{2+} induce spectral changes similar to those observed for Cu^{2+}. However, in the case of compound **4** a more intense band at 450 nm was observed, suggesting a higher affinity of compound **4** for Fe^{2+} towards Cu^{2+} (see Fig. S15). Despite in the same order, the association constant of **4** is higher for Fe^{2+} (6.62 ± 0.03; 1:1 (L:M)) than for Cu^{2+} (6.25 ± 0.04; 1:1 (L:M)).

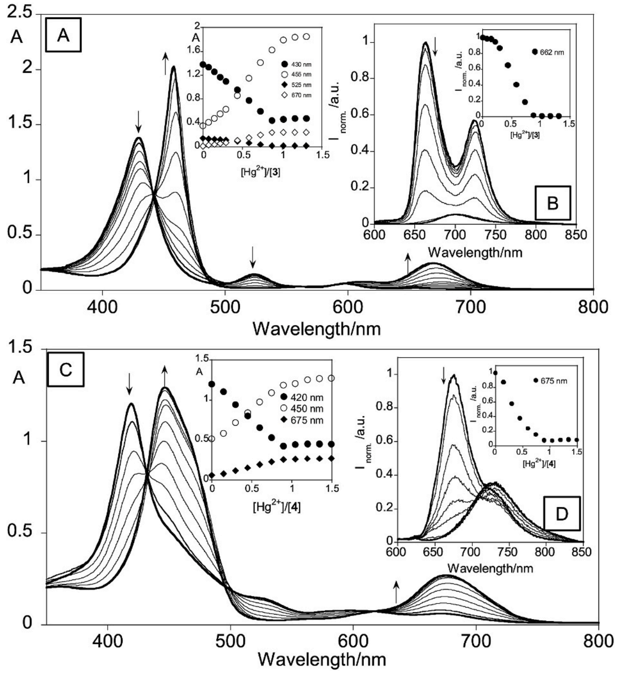

Fig. 4. Spectrophotometric (A, C) and spectrofluorimetric (B, D) titrations of compound **3** (A, B) and **4** (C,D) with the addition of Hg^{2+} in dichloromethane. The inset represents the absorption (A, C) at 430 nm, 455 nm, 525 nm, 670 nm for (A) and 420 nm, 530 nm, 675 nm for (C); and the emission intensity (B, D) at 662 nm (B) and 675 nm (D), as function of $[Hg^{2+}]/[\mathbf{3}]$ (A, B) and $[Hg^{2+}]/[\mathbf{4}]$ (C, D). ($[\mathbf{3}]$, $[\mathbf{4}] = 1 \times 10^{-5}$ M, $\lambda_{exc3} = 525$ nm, $\lambda_{exc4} = 530$ nm, T = 298 K).

3.3.3. Hg^{2+} and Cd^{2+} metal ions

The Hg^{2+} ion is considered one of the most toxic metal ions because of its inorganic form that can be converted by bacteria into the highly toxic methylmercury. As a heavy metal ion, Hg^{2+} acts as a fluorescence quencher *via* a spin-orbit coupling effect producing a turn-off mechanism in most sensing systems [44,45]. The addition of Hg^{2+} induces, for both porphyrin derivatives (**3** and **4**), a red shift of the Soret band from 420-430 nm to 450–455 nm, as well as the appearance of a new band at 670–675 nm. In the excited state, it was possible to observe a decrease in the emission signal at the bands 662–675 nm Q (0-0) and *ca.* 730 nm Q (0-0) (0–1). These modifications are indicative of metal complexation. In Fig. 4 the absorption titrations of porphyrins **3** and **4** with Hg^{2+} are shown. Similar behaviour was observed for Cd^{2+} metal (Fig. S16). The highest association constants were obtained for Hg^{2+}, with values of Log $K_{ass} = 7.75 \pm 0.02$ (1:1) for **3** and Log $K_{ass} = 7.38 \pm 0.04$ (1:1) for **4**, with a stoichiometry of 1:1 (L: M).

3.3.4. Co^{2+}, Ni^{2+} and Ag^{+} metal ions

To complete the interaction of compounds **3** and **4** with the most biological important transition metal ions, the titrations with Co^{2+}, Ni^{2+} and Ag^{+} with compounds **3** and **4** were studied. In all cases lead to similar spectral alterations to the ones obtained for Zn^{2+}, Cu^{2+}, Fe^{2+}, Cd^{2+} and Hg^{2+}, as it can be seen in Figs. S17–S19. All titrations showed spectral evidence of the porphyrin inner core coordination by the metal ions. The stability constants reveal the formation of mononuclear species, where the sequence obtained for **3** and **4** decreases in the following order: $Ni^{2+}>Co^{2+}>Ag^{+}$ for **3** and $Co^{2+}>Ni^{2+}>Ag^{+}$ for **4**.

From the overall point of view, the final sequence of the strongest interaction obtained was $Hg^{2+}>Cu^{2+}>Zn^{2+}>Fe^{2+}>Cd^{2+}>Ni^{2+}>Co^{2+}>Ag^{+}$ for **3** and $Cd^{2+}\approx Hg^{2+}>Co^{2+}>Zn^{2+}>Fe^{2+}>Cu^{2+}>Ni^{2+}>Ag^{+}$ for **4**.

Concerning the sensorial ability of compounds **3** and **4** towards the studied metal ions and future application of these probes, the detection (LOD) and quantification (LOQ) limits were also determined at 670 nm

(**3**) and 675 nm (**4**) by absorption (see Table 2). It was determined the values of LOD = 0.025 ± 0.003/LOQ = 0.041 ± 0.05 for **3** and LOD = 0.061 ± 0.004/LOQ = 0.084 ± 0.006 for **4**. The minimal detectable and quantified amounts for all studies metal ions were also determined, and the values are listed in Table 2. From the results obtained it was possible to conclude that both compounds are able to detect and quantify the fewest amount of the Hg^{2+} toxic metal ion of 0.9/5.3 μM and 1.8/3.6 μM for compound **3** and **4**, respectively.

3.4. *PMMA films for sensing applications*

In order to increase the analytical applications of porphyrin derivatives **3** and **4**, several low-cost polymeric PMMA-doped samples were prepared and studied towards Zn^{2+}, Cd^{2+} and Hg^{2+} metal ions, and as a function of the temperature. PMMA has been selected as the host matrix being already investigated with good results in our research team for similar sensing [14]. Films in PMMA with 0.25–1.5% w/w of the dyes **3**, **4** were obtained using a polymer amount of 100 mg. For the solid-state temperature assays, PMMA films with 0.5–3.0% of **TPP** and **ZnTPP** were also prepared for comparison. In Fig. 5 the obtained composite films containing the 0.25–3.0% of the dyes are reported.

Three replicates of the same sample were obtained in order to verify the reproducibility of the film production. The PMMA_**4** films did not show a reasonable degree of homogeneity for all range of dye concentration investigated; this suggests a partial incompatibility between the polymeric matrix and the dye that determines the migration and aggregation of the dye during the evaporation of the solvent giving differently coloured areas on the film surface.

The PMMA_**3** films, on the other hand, showed a more homogeneous surface even at the highest dye content thus suggesting effective dye/polymer interactions that, in turn, favored a good reproducibility in film formation.

Also, **TPP** and **Zn-TPP** dyes showed a high degree of compatibility with the PMMA host matrix in agreement with literature reports [14, 46]. Among all replicas, the samples showing the most homogeneous surface were utilized for the successive sensing studies.

3.4.1. *Sensing of metal ions: solid-state*

Based on the good results obtained in solution, solid thin films doped with different dye concentrations are prepared in order to evaluate the possibility to replicate this sensing behaviour also in solid-state.

With this purpose, water solutions of the metal ions of interest (Hg^{2+}, Cd^{2+} and Zn^{2+}) were prepared at different metal concentrations (0, 2.5 and 30 ppm). The films previously obtained were immersed for 5 min in the different solutions at growing concentrations of metal ion, and the emission spectra were then collected in order to evaluate the interaction between the metal ion and the considered dye dispersed in a PMMA thin film.

Table 2
Minimal detection (LOD) and quantification (LOQ) amounts (μM) of studied metal ions (M) by compounds **3** and **4**. [LOD and LOQ were measured by absorption at 670 and 675 nm for **3** and **4**, respectively].

Compounds (L)	Metal (M)	LOD (μM)	LOQ (μM)
3	Zn^{2+}	2.9	8.7
	Cd^{2+}	5.3	13.1
	Co^{2+}	5.6	53.2
	Fe^{2+}	2.8	8.5
	Ni^{2+}	2.5	12.5
	Cu^{2+}	5.0	8.3
	Hg^{2+}	0.9	5.3
	Ag^{+}	11.9	110.4
4	Zn^{2+}	4.4	5.8
	Cd^{2+}	5.3	7.9
	Co^{2+}	2.8	5.6
	Fe^{2+}	2.8	5.7
	Ni^{2+}	2.5	7.5
	Cu^{2+}	6.6	10.0
	Hg^{2+}	1.8	3.6
	Ag^{+}	11.9	17.9

The interaction between the metal ions and the samples containing the dye **3** do not show a significant cation sensing effect (data not shown). However, in the case of metal ions Hg^{2+} and Zn^{2+} it was observed a slight decrease of *ca.*10% of the peak's intensity in absorption and emission response when the concentration of the metal ions is 30 ppm (data not shown). This is probably due to the fact that only very weak interactions are established between the cations and the dye molecules exposed on the surface of the thin sample. This result could have been expected since PMMA is not water-soluble and therefore, only limited interaction with the dyes distributed close to the matrix surface can occur. Nevertheless, the segregation of dye molecules at the air/polymer film contact surface is reasonable to occur because solvent evaporation progressively distributes them during film formation [47].

Analogous outcomes were gathered for polymer samples containing the dye **4**.

3.4.2. *Physical sensing: solid-state temperature sensing*

The PMMA-based doped film with the compounds **TPP**, **ZnTPP**, **3** and **4** was cut into pieces in order to be used for verifying eventual thermal sensing capability.

In order to determine their potential use as thermal sensors, the prepared 10 × 10 × 0.09 mm dye-doped films were placed on a heating plate. The emission spectra were recorded at the variation of the temperature from 25 to 100 °C and from 100 to 35 °C in order to verify if the temperature sensing was reversible.

Fig. 6 and S20 shows the emission spectra of the PMMA polymers doped with dyes **3**, **4**, **TPP** and **ZnTPP**, (1.5%). Temperature increasing (from 25 °C to 100 °C) lead to a reduction of the emission intensity for all doped polymers. Such phenomenon is typical for porphyrins and can be explained by the thermal quenching effect [48].

Noteworthy, in the cooling phase (from 100 °C to 35 °C), PMMA_**3** and PMMA_**4** showed a recovery of emission intensity of *ca.* 70–80%. Similar spectra changes were observed for the other percentages of dyes (0.25% and 0.5%) for PMMA_**3** and PMMA_**4**. On the other hand, for PMMA_**TPP** and PMMA_**ZnTPP** polymer films such recovery is not observed, indicating that the temperature solicitation possibly induced a permanent modification of the dye distribution within the PMMA matrix. This phenomenon can be addressed the presence of weak **TPP**/**ZnTPP**/polymer interactions that can be easily destroyed by temperature thus promoting the formation of poorly emissive porphyrinic aggregates. Conversely, the lateral functionalization of **TPP** in **3** and **4** chromophores possibly increased the number of effective interactions with the acrylate moieties of PMMA and also reducing the overall planarity of the dye that could promote the formation of aggregated stacked structures within the solid polymer matrix [49].

Among all the samples, the PMMA_**3** shows the best performances as temperature optical probe in the range 25–100 °C. Indeed, its optical properties are practically full recovered after the temperature measurement cycle.

These preliminarily results gathered from PMMA_**3** and PMMA_**4** are quite promising for the development of low cost temperature indicators for smart plastic labels.

4. Conclusion

Porphyrin derivatives **3** and **4** were successfully synthesized and characterized. Porphyrin **3** showed a fluorescent quantum yield higher than **4** (*ca.* 10 times), which could be related to the spacer increase of the chain in the beta position. Such an increase could lead to a decrease in the planarity of molecule leading then to a less emissive compound (**4**). Concerning the sensorial ability of compound **3** and **4**, spectral changes in ground and excited state were observed for both compounds. The observed spectral changes are related to the complexation of the

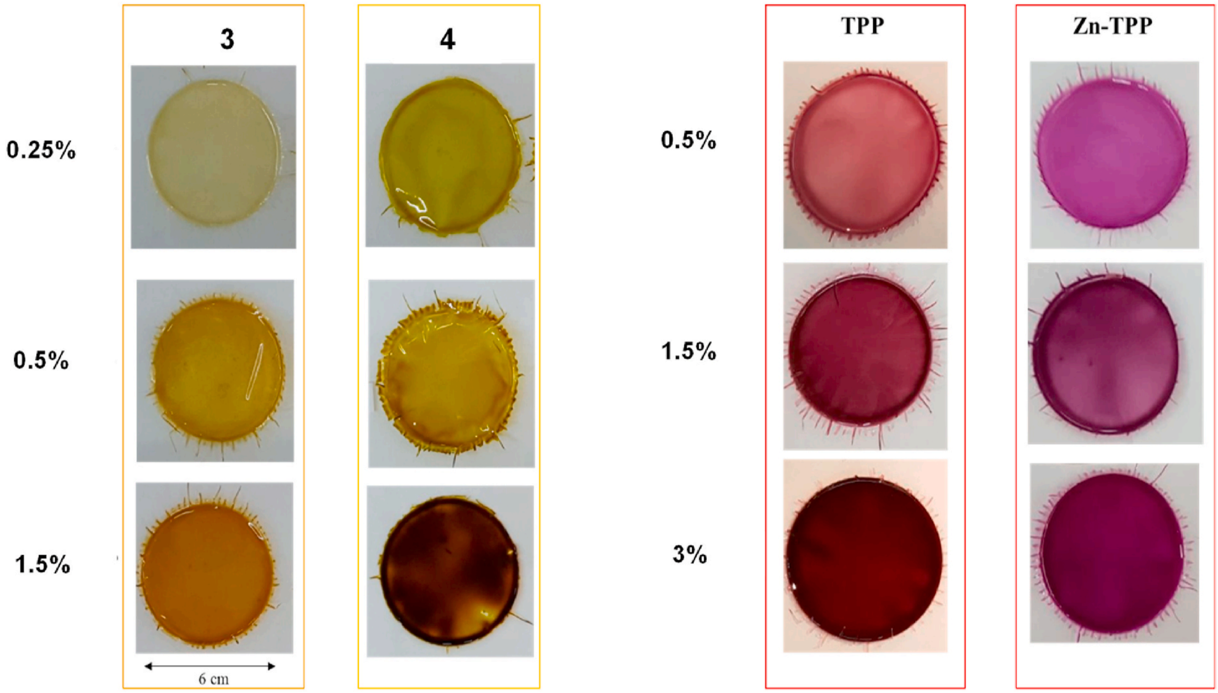

Fig. 5. PMMA films doped with **TPP**, **ZnTPP**, **3** and **4**.

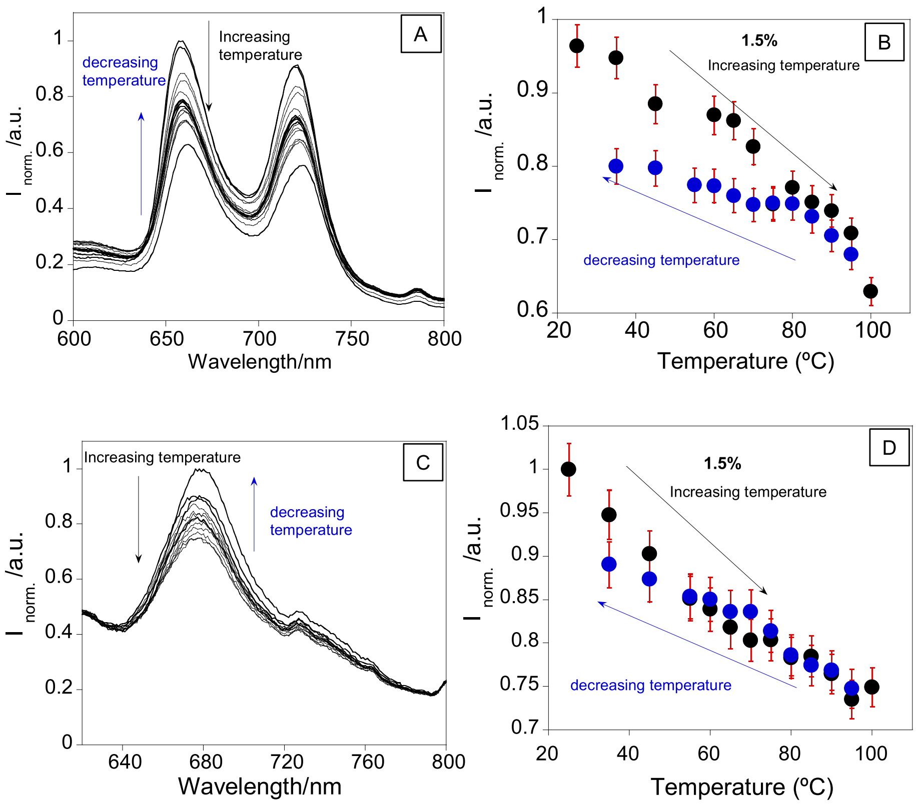

Fig. 6. Emission spectra of samples PMMA_**3** (1.5%) (A) and PMMA_**4** (1.5%) (C). Emission intensities at 659 nm (B) and 678 nm (D) as a function of temperature for PMMA_**3** (1.5%) (A) and PMMA_**4** (1.5%), respectively.

porphyrin macrocycle by the metal ions. In the same way, upon complexation, a colour change from pale yellow to green was detected. The results indicate a ligand-to-metal complex stoichiometry of 1:1. In particular, compound **3** showed the best results for Hg^{2+} metal ions. Preliminarily results gathered from PMMA films doped with **3** and **4**, indicated promising results as temperature optical probes when compared with the non-substituted derivatives **TPP** and **ZnTPP**. PMMA_**3** revels to be the best candidate showing reversible optical properties in function of temperature, with the recovery of *ca.* 80% in the cooling phase.

CRediT authorship contribution statement

Nuno M.M. Moura: Conceptualization, Methodology, Validation, Investigation, Resources, Data curation, Writing - original draft, Writing - review & editing, Visualization, Supervision, Project administration. **Simone Valentini:** Validation, Investigation, Data curation, Visualization. **Victoria Cheptene:** Validation, Data curation, Investigation. **Andrea Pucci:** Conceptualization, Methodology, Resources, Supervision, Writing - original draft, Writing - review & editing, Funding acquisition. **M. Graça P.M.S. Neves:** Conceptualization, Methodology, Resources, Supervision, Writing - original draft, Writing - review & editing, Funding acquisition. **José Luis Capelo:** Resources, Writing - original draft, Writing - review & editing, Funding acquisition. **Carlos Lodeiro:** Conceptualization, Methodology, Resources, Writing - original draft, Writing - review & editing, Funding acquisition, Supervision. **Elisabete Oliveira:** Conceptualization, Methodology, Validation, Investigation, Resources, Data curation, Writing - original draft, Writing - review & editing, Visualization, Supervision, Project administration.

Declaration of competing interest

The authors declare that they have no known competing financial interests or personal relationships that could have appeared to influence the work reported in this paper.

Acknowledgments

EO and CL thank the financial support by Associate Laboratory for Green Chemistry - LAQV which is financed by national funds from FCT/MCTES (UIDB/50006/2020), as well as the Scientific Society PROTEOMASS (Portugal) for funding support (General Funding Grants 2018 and 2019). E.O thanks FCT/MEC (Portugal) for the individual contract, CEECIND/00648/2017.

The authors are grateful to University of Aveiro and FCT/MCT for the financial support for QOPNA research Unit (FCT UID/QUI/00062/2019) and the LAQV (UIDB/50006/2020) through national funds and, where applicable, co-financed by the FEDER, within the PT2020 Partnership Agreement, and to the Portuguese NMR Network. The research contract of N.M.M. Moura (REF.-048-88-ARH/2018) is funded by national funds (OE), through FCT – Fundação para a Ciência e a Tecnologia, I.P., in the scope of the framework contract foreseen in the numbers 4, 5 and 6 of the article 23, of the Decree-Law 57/2016, of August 29, changed by Law 57/2017, of July 19.

SV and VC would like to acknowledge the Erasmus exchange program for the financial support in their exchange programme between the University of Pisa (Italy) and the NOVA University Lisbon (Portugal).

Appendix A. Supplementary data

Supplementary data to this article can be found online at https://doi.org/10.1016/j.dyepig.2020.108897.

References

[1] Lee H, Hong K-I, Jang W-D. Design and applications of molecular probes containing porphyrin derivatives. Coord Chem Rev 2018;354:46–73. https://doi.org/10.1016/j.ccr.2017.06.008.

[2] Paolesse R, Nardis S, Monti D, Stefanelli M, Di Natale C. Porphyrinoids for chemical sensor applications. Chem Rev 2017;117:2517–83. https://doi.org/10.1021/acs.chemrev.6b00361.

[3] Pellegrin Y, Odobel F. Molecular devices featuring sequential photoinduced charge separations for the storage of multiple redox equivalents. Coord Chem Rev 2011;255:2578–93. https://doi.org/10.1016/j.ccr.2010.12.017.

[4] Percástegui EG, Jancik V. Coordination-driven assemblies based on meso-substituted porphyrins: metal-organic cages and a new type of meso-metallaporphyrin macrocycles. Coord Chem Rev 2020;407:213165. https://doi.org/10.1016/j.ccr.2019.213165.

[5] Moreira X, Santos P, Faustino MAF, Raposo MMM, Costa SPG, Moura NMM, et al. An insight into the synthesis of cationic porphyrin-imidazole derivatives and their photodynamic inactivation efficiency against Escherichia coli. Dyes Pigments 2020;178:108330. https://doi.org/10.1016/j.dyepig.2020.108330.

[6] Dias CJ, Sardo I, Moura NMM, Felgueiras J, Neves MGPMS, Fardilha M, et al. An efficient synthetic access to new uracil-alditols bearing a porphyrin unit and biological assessment in prostate cancer cells. Dyes Pigments 2020;173:107996. https://doi.org/10.1016/j.dyepig.2019.107996.

[7] Moura NMM, Esteves M, Vieira C, Rocha GMSRO, Faustino MAF, Almeida A, et al. Novel β-functionalized mono-charged porphyrinic derivatives: synthesis and photoinactivation of Escherichia coli. Dyes Pigments 2019;160:361–71. https://doi.org/10.1016/j.dyepig.2018.06.048.

[8] Beletskaya I, Tyurin VS, Tsivadze AY, Guilard R, Stern C. Supramolecular Chemistry of metalloporphyrins. Chem Rev 2009;109:1659–713. https://doi.org/10.1021/cr800247a.

[9] Liu B-W, Chen Y, Song B-E, Liu Y. Amphiphilic porphyrin assembly as a highly selective chemosensor for organic mercury in water. Chem Commun 2011;47:4418. https://doi.org/10.1039/c0cc05413e.

[10] Zhu M, Zhou Y, Yang L, Li L, Qi D, Bai M, et al. Synergistic coupling of fluorescent "turn-off" with spectral overlap modulated FRET for ratiometric Ag + sensor. Inorg Chem 2014;53:12186–90. https://doi.org/10.1021/ic502141q.

[11] Choi JK, Sargsyan G, Olive AM, Balaz M. Highly sensitive and selective spectroscopic detection of mercury(II) in water by using pyridylporphyrin-DNA conjugates. Chem Eur J 2013;19:2515–22. https://doi.org/10.1002/chem.201202461.

[12] Moura NMM, Nunez C, Faustino MAF, Cavaleiro JAS, Neves MGPMS, Capelo JL, et al. Preparation and ion recognition features of porphyrin-chalcone type compounds as efficient red-fluorescent materials. J Mater Chem C 2014;2:4772–83. https://doi.org/10.1039/C3TC32496F.

[13] Moura NMM, Núñez C, Santos SM, Faustino MAF, Cavaleiro JAS, Neves MGPMS, et al. Synthesis, spectroscopy studies, and theoretical calculations of new fluorescent probes based on pyrazole containing porphyrins for Zn(II), Cd(II), and Hg(II) optical detection. Inorg Chem 2014;53:6149–58. https://doi.org/10.1021/ic500634y.

[14] Moura NMM, Nuñez C, Santos SM, Faustino MAF, Cavaleiro JAS, Neves MGPMS, et al. Functionalized porphyrins as red fluorescent probes for metal cations: spectroscopic, MALDI-TOF spectrometry, and doped-polymer studies. Chempluschem 2013;78:1230–43. https://doi.org/10.1002/cplu.201300216.

[15] Moura NMM, Núñez C, Santos SM, Faustino MAF, Cavaleiro JAS, Almeida Paz FA, et al. A new 3,5-bisporphyrinylpyridine derivative as a fluorescent ratiometric probe for zinc ions. Chem Eur J 2014;20:6684–92. https://doi.org/10.1002/chem.201402270.

[16] Zhang X-B, Guo C-C, Li Z-Z, Shen G-L, Yu R-Q. An optical fiber chemical sensor for mercury ions based on a porphyrin dimer. Anal Chem 2002;74:821–5. https://doi.org/10.1021/ac0109218.

[17] Yang Y, Jiang J, Shen G, Yu R. An optical sensor for mercury ion based on the fluorescence quenching of tetra(p-dimethylaminophenyl)porphyrin. Anal Chim Acta 2009;636:83–8. https://doi.org/10.1016/j.aca.2009.01.038.

[18] Liu X, Liu X, Tao M, Zhang W. A highly selective and sensitive recyclable colorimetric Hg 2+ sensor based on the porphyrin-functionalized polyacrylonitrile fiber. J Mater Chem 2015;3:13254–62. https://doi.org/10.1039/C5TA02491A.

[19] Chen Y-Z, Jiang H-L. Porphyrinic metal–organic framework catalyzed heck-reaction: fluorescence "turn-on" sensing of Cu(II) ion. Chem Mater 2016;28:6698–704. https://doi.org/10.1021/acs.chemmater.6b03030.

[20] Liu C, Liang X, Liu J, Liu Y, Luo J, Zhu H. Efficient removal of Cd(<scp>ii</scp>) ions from aqueous solutions via visible capturing. RSC Adv 2016;6:38430–6. https://doi.org/10.1039/C6RA03103J.

[21] Tsuda A, Sakamoto S, Yamaguchi K, Aida T. A novel supramolecular multicolor thermometer by self-assembly of a π -extended zinc porphyrin complex. J Am Chem Soc 2003;125:15722–3. https://doi.org/10.1021/ja038349k.

[22] Yan Q, Yuan J, Kang Y, Cai Z, Zhou L, Yin Y. Dual-sensing porphyrin-containing copolymer nanosensor as full-spectrum colorimeter and ultra-sensitive thermometer. Chem Commun 2010;46:2781. https://doi.org/10.1039/b926882k.

[23] Armarego WLF, Chai C. Purification of laboratory chemicals. seventh ed. Oxford: Butterworth-Heinemann; 2013.

[24] Adler AD, Longo FR, Shergalis W. Mechanistic investigations of porphyrin syntheses. I. Preliminary studies on ms -tetraphenylporphin. J Am Chem Soc 1964;86:3145–9. https://doi.org/10.1021/ja01069a035.

[25] Adler AD, Longo FR, Finarelli JD, Goldmacher J, Assour J, Korsakoff L. A simplified synthesis for meso-tetraphenylporphine. J Org Chem 1967;32:476. https://doi.org/10.1021/jo01288a053. 476.

[26] Gonsalves AM d'AR, Varejão JMTB, Pereira MM. Some new aspects related to the synthesis of meso -substituted porphyrins. J Heterocycl Chem 1991;28:635–40. https://doi.org/10.1002/jhet.5570280317.

[27] Buchler JW, Smit KM. Porphyrins and metalloporphyrins. Amesterdam: Elsevier; 1975.

[28] Moura NMM, Ramos CIV, Linhares I, Santos SM, Faustino MAF, Almeida A, et al. Synthesis, characterization and biological evaluation of cationic porphyrin–terpyridine derivatives. RSC Adv 2016;6:110674–85. https://doi.org/10.1039/C6RA25373C.

[29] Ramos CIV, Moura NMM, Santos SMF, Faustino MA, Tomé JPC, Amado FML, et al. An insight into the gas-phase fragmentations of potential molecular sensors with porphyrin-chalcone structures. Int J Mass Spectrom 2015;392:164–72. https://doi.org/10.1016/j.ijms.2015.10.008.

[30] Berlman IB, Berlman IB, Berlman IB. Handbook of fluorescence spectra of aromatic molecules. second ed. New York: Academic Press; 1971. NY.

[31] Montalti M, Credi A, Prodi Mg L, Montalti M, Credi A, Prodi LGM. Handbook of photochemistry. third ed. Boca Raton: BOCA: Taylor & Francis; 2006.

[32] Moura NMM, Faustino MAF, Neves MGPMS, Duarte AC, Cavaleiro JAS. Vilsmeier-Haack formylation of Cu(II) and Ni(II) porphyrin complexes under microwaves irradiation. J Porphyr Phthalocyanines 2011;15:652–8. https://doi.org/10.1142/S1088424611003586.

[33] Santos CIMM, Oliveira E, Menezes J, Barata JFB, Faustino MAF, Ferreira VF, et al. New coumarin–corrole and –porphyrin conjugate multifunctional probes for anionic or cationic interactions: synthesis, spectroscopy, and solid supported studies. Tetrahedron 2014;70:3361–70. https://doi.org/10.1016/j.tet.2013.07.022.

[34] Spellane PJ, Gouterman M, Antipas A, Kim S, Liu YC. Porphyrins. 40. Electronic spectra and four-orbital energies of free-base, zinc, copper, and palladium tetrakis (perfluorophenyl)porphyrins. Inorg Chem 1980;19:386–91. https://doi.org/10.1021/ic50204a021.

[35] Gouterman M. Optical spectra and electronic structure of porphyrins and related rings. The Porphyrins, Elsevier; 1978. p. 1–165. https://doi.org/10.1016/B978-0-12-220103-5.50008-8.

[36] Rasouli S, Sakha F, Mojarrad AG, Zakavi S. Thermal nonlinear optical response of meso-tetraphenylporphyrin under aggregation conditions versus that in the absence of aggregation. J Mod Optic 2018;65:1009–17. https://doi.org/10.1080/09500340.2017.1418442.

[37] Gans P, Sabatini A, Vacca A. Investigation of equilibria in solution. Determination of equilibrium constants with the HYPERQUAD suite of programs. Talanta 1996; 43:1739–53. https://doi.org/10.1016/0039-9140(96)01958-3.

[38] Fleischer EB, Dixon F. Definitive evidence for the existence of the “sitting-atop” porphyrin complexes in nonaqueous solutions. Bioinorg Chem 1977;7:129–39. https://doi.org/10.1016/S0006-3061(00)80063-0.

[39] De Luca G, Romeo A, Scolaro LM, Ricciardi G, Rosa A. Sitting-atop metallo-porphyrin complexes: experimental and theoretical investigations on such elusive species. Inorg Chem 2009;48:8493–507. https://doi.org/10.1021/ic9012153.

[40] Radi S, Abiad C El, Moura NMM, Faustino MAF, Neves MGPMS. New hybrid adsorbent based on porphyrin functionalized silica for heavy metals removal: synthesis, characterization, isotherms, kinetics and thermodynamics studies. J Hazard Mater 2019;370:80–90. https://doi.org/10.1016/j.jhazmat.2017.10.058.

[41] Han ZX, Luo HY, Zhang XB, Kong RM, Shen GL, Yu RQ. A ratiometric chemosensor for fluorescent determination of Hg2+ based on a new porphyrin-quinoline dyad. Spectrochim Acta Part A Mol Biomol Spectrosc 2009;72:1084–8. https://doi.org/10.1016/j.saa.2009.01.003.

[42] Yang W, Chen X, Su H, Fang W, Zhang Y. The fluorescence regulation mechanism of the paramagnetic metal in a biological HNO sensor. Chem Commun 2015;51: 9616–9. https://doi.org/10.1039/C5CC00787A.

[43] Morais NA, Fernandes L, Ariana-Machado J, Capelo JL, Lodeiro C, Oliveira E. An unusual emissive and colorimetric copper (II) detection by a selective probe based on a pseudo-crown cysteine dye: solution and gas phase studies. Inorg Chem Commun 2017;86:299–303. https://doi.org/10.1016/j.inoche.2017.11.001.

[44] Pinheiro D, De Castro CS, Seixas De Melo JS, Oliveira E, Nunez C, Fernandez-Lodeiro A, et al. From yellow to pink using a fluorimetric and colorimetric pyrene derivative and mercury (II) ions. Dyes Pigments 2014;110:152–8. https://doi.org/10.1016/j.dyepig.2014.04.012.

[45] Oliveira E, Lorenzo J, Cid A, Capelo JLJL, Lodeiro C. Non-toxic fluorescent alanine–fluorescein probe with green emission for dual colorimetric/fluorimetric sensing. J Photochem Photobiol Chem 2013;269:17–26. https://doi.org/10.1016/j.jphotochem.2013.06.015.

[46] Costa JIT, Oliveira E, Santos HM, Tomé AC, Neves MGPMS, Lodeiro C. Study of multiporphyrin compounds as colorimetric sitting-atop metal complexes: synthesis and photophysical studies. Chempluschem 2016;81:143–53. https://doi.org/10.1002/cplu.201500386.

[47] Martini G, Martinelli E, Ruggeri G, Galli G, Pucci A. Julolidine fluorescent molecular rotors as vapour sensing probes in polystyrene films. Dyes Pigments 2015;113:47–54. https://doi.org/10.1016/j.dyepig.2014.07.025.

[48] Kolesnikov IE, Kalinichev AA, Kurochkin MA, Kolesnikov EY, Lähderanta E. Porphyrins as efficient ratiometric and lifetime-based contactless optical thermometers. Mater Des 2019;184:108188. https://doi.org/10.1016/j.matdes.2019.108188.

[49] Pucci A, Tirelli N, Ruggeri G, Ciardelli F. Absorption and emission dichroism of polyethylene films with molecularly dispersed push-pull terthiophenes. Macromol Chem Phys 2005;206:102–11. https://doi.org/10.1002/macp.200400171.